J. Fluid Mech. (2001), *vol.* 448, *pp.* 279–288.
DOI: 10.1017/S0022112001006176 Printed in the United Kingdom

Anisotropy of small-scale scalar turbulence

By SUSAN KURIEN[1], KONSTANTINOS G. AIVALIS[2] AND KATEPALLI R. SREENIVASAN[1,2]

[1]Department of Physics, Yale University, New Haven, CT 06520, USA

[2]Department of Mechanical Engineering, Yale University, New Haven, CT 06520, USA

(Received 20 August 2001)

The anisotropy of small-scale temperature fluctuations in shear flows is analysed by making measurements in high-Reynolds-number atmospheric surface layers. A spherical harmonics representation of the moments of scalar increments is proposed, such that the isotropic part corresponds to the index $j = 0$ and increasing degrees of anisotropy correspond to increasing j. The parity and angular dependence of the odd moments of the scalar increments show that the moments cannot contain any isotropic part ($j = 0$), but can be satisfactorily represented by the lowest-order anisotropic term corresponding to $j = 1$. Thus, the skewnesses of scalar increments (and derivatives) are inherently anisotropic quantities, and are not suitable indicators of the tendency towards isotropy.

1. Introduction

Let θ be a scalar advected passively by a turbulent shear flow. The postulate of local isotropy, or the statistical isotropy of small scales, demands that odd moments of a spatial derivative $\partial\theta/\partial x$ (say) should vanish: derivatives are small-scale quantities and isotropy in this instance subsumes reflectional symmetry. In practice, as the turbulence Reynolds number increases and conditions become increasingly favourable for local isotropy to prevail, the derivative skewness $S = \langle(\partial\theta/\partial x)^3\rangle/\langle(\partial\theta/\partial x)^2\rangle^{3/2}$ should approach zero rapidly. Instead, it remains $O(1)$ for all Reynolds numbers for which measurements are now available; such measurements extend up to Taylor microscale Reynolds numbers of 2×10^4 (see figure 1 reproduced from Sreenivasan & Antonia 1997). Similarly, the skewness of the temperature increment across a scale $\boldsymbol{r}$, $\langle(\theta(\boldsymbol{x}+\boldsymbol{r}) - \theta(\boldsymbol{x}))^3\rangle/\langle(\theta(\boldsymbol{x}+\boldsymbol{r}) - \theta(\boldsymbol{x}))^2\rangle^{3/2}$, is expected, by local homogeneity and isotropy, to be zero for small $|\boldsymbol{r}|$, or to decrease rapidly with diminishing scale $|\boldsymbol{r}|$. Measurements show that this increment skewness remains $O(1)$, essentially independent of the separation scale (see figure 2). For these two reasons, it has been appreciated for some time (see, for example, Sreenivasan 1991 and Warhaft 2000 for recent reviews) that, in the presence of a mean gradient, the passive scalar is persistently anisotropic even at the smallest scales at very high Reynolds numbers. This is then an indication that local isotropy, and the associated picture of universality of small scales, may need to be modified significantly if it is to survive as an underpinning of turbulence theory.

That a residual anisotropy also exists in the turbulent velocity field is now evident from the high-Reynolds-number measurements of Mydlarski & Warhaft (1998), Shen & Warhaft (2000) and Kurien & Sreenivasan (2000), to cite just three references. Recently, Arad *et al.* (1998, 1999*a*), Kurien *et al.* 2000, Kurien & Sreenivasan (2001),

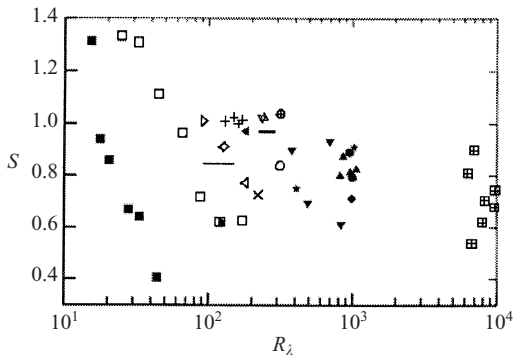

FIGURE 1. The magnitude of the skewness of the temperature derivative for a range of Reynolds numbers, where the Taylor microscale Reynolds number $R_\lambda = u'\lambda/\nu$, u' is the mean-square velocity, λ the Taylor microscale, and ν the fluid viscosity. The plot is a reproduction of figure 7 in Sreenivasan & Antonia (1997), where the individual sources of data are stated. In the low to modest R_λ range, the data come from laboratory experiments and direct numerical simulations, while those on the high end come from atmospheric measurements.

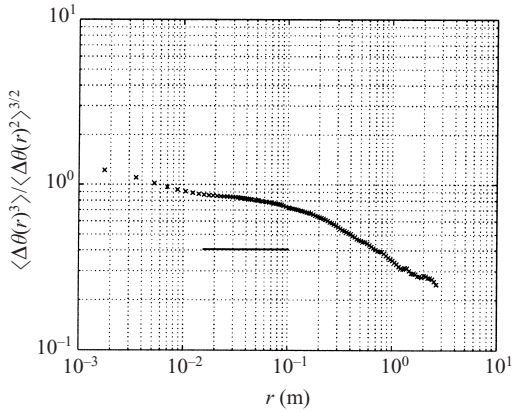

FIGURE 2. The skewness of the temperature increments in the atmospheric boundary layer at 9.5 cm above the ground; the Taylor microscale Reynolds number is about 2000. The horizontal dark line is the span of the inertial range, determined by the linear range of the third-order velocity structure function.

Grossmann, von der Heydt & Lohse (2001) and Biferale & Vergassola (2001) have used new techniques for characterizing the anisotropy in the velocity field and for separating the isotropic and anisotropic parts of statistical objects such as structure functions. The techniques use the irreducible representation of the SO(3) symmetry group. The conclusion from these studies is essentially that, in the hierarchical representation of the SO(3) group, the ratio of the anisotropic part to the isotropic part diminishes with decreasing scale *for structure functions of any given order* – albeit more slowly than expected from dimensional considerations (e.g. Lumley 1967). This conclusion provides a richer perspective on local isotropy and removes, to some degree, the problems associated with its apparent violation for the velocity field. Our goal here is to apply the SO(3) methodology for the passive scalar field, and assess if similar conclusions hold. For the scalar case, the SO(3) representation reduces to a standard spherical harmonics expansion.

Section 2 discusses new measurements and is followed by a description of the

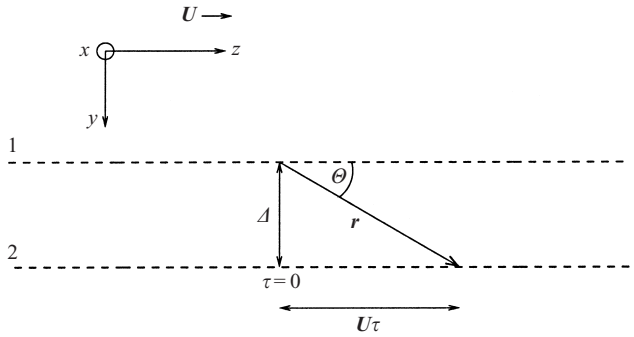

FIGURE 3. Schematic of the experimental setup as seen from above. The two probes are denoted by 1 and 2. The mean wind $\boldsymbol{U}$ is oriented along the z-axis (see text). The probes are separated by a fixed distance $\Delta = 0.05$ m along the y-axis and oriented orthogonal to $\boldsymbol{U}$. The remaining coordinate x points out of the plane. The use of Taylor's hypothesis gives two lines of the temperature signal indicated by the dashed lines in space, one for each probe. The correlation between signals from the two probes may be calculated for a separation $\boldsymbol{r}$ with magnitude $r = \sqrt{\Delta^2 + (U\tau)^2}$.

analytical tools in § 3. Section 4 shows that the isotropic part of the spherical harmonics representation cannot contribute to the skewness of temperature increments and derivatives, and that at least the lowest-order anisotropy is required to describe the observed parity and spatial dependence. The implications of these results are discussed in § 5.

2. New measurements

The nth-order structure function of temperature is given by

$$T^{(n)}(\boldsymbol{r}) = \langle(\theta(\boldsymbol{x}+\boldsymbol{r}) - \theta(\boldsymbol{x}))^n\rangle, \tag{2.1}$$

where $\langle\cdot\rangle$ denotes spatial averaging over the vector coordinate $\boldsymbol{x}$, and $\boldsymbol{r}$ is the vectorial scale separation. This is the object of interest here, particularly the case $n = 3$. In most previous measurements, Taylor's hypothesis has been assumed and spatial separation has been considered only in the direction of the mean wind. That is, the spatial separation is a scalar in the direction of the mean wind U, given by $U\tau$, where τ the time increment in a single-point temperature θ. Taylor's hypothesis does not alter the conclusion that anisotropy exists (see e.g. Mi & Antonia 1994). However, restricting the separation distance to one preferred direction hides the angular dependence of the structure function, which makes it impossible to explore that aspect of anisotropy. We can improve this situation in a simple way, as described below.

Define a coordinate system in which (for convenience) the z-axis is in the direction of the mean wind, the x-axis is vertical and the y-axis (to be called the spanwise direction) is orthogonal to x and z. Figure 3 provides a schematic. We measure the temperature at two points separated by a fixed spanwise distance Δ. For both probes, the mean wind is essentially the same. Denoting the two probes by subscripts 1 and 2, we construct the structure function

$$T^{(n)}(r, \Theta, \Phi) = \langle(\theta_2(t+\tau) - \theta_1(t))^n\rangle, \tag{2.2}$$

where $r = \sqrt{\Delta^2 + (U\tau)^2}$, Θ is the polar angle with respect to the mean-wind direction z, given by $\sin\Theta = \Delta/r$ and the azimuthal angle $\Phi = \pi/2$ for this particular geometry. This configuration allows the structure function to vary with the magnitude and the

direction of the scale separation vector $\boldsymbol{r}$. This additional freedom, albeit constrained by the condition $r \sin \Theta = \Delta$, is achieved by the application of Taylor's hypothesis to temperature signals from one or both probes.

Measurements were made in the boundary layer above the salt flats of the Dugway Proving Grounds in Utah, at a height h of 1.75 m above the ground. The ground was smooth on the order of a millimetre. Measurements were made between 1720 hours and 2100 hours during a summer day of the year 2000. The wind was essentially steady in magnitude and direction over this duration. We arranged the data into four sets, I–IV. The wind speed, determined from independent measurements using a Pitot tube mounted nearby, was $3\,\mathrm{m\,s^{-1}}$ for set I and $3.5\,\mathrm{m\,s^{-1}}$ for sets II–IV. For set I, obtained between 1720 and 1800 hours, the ground was on the average about 4 K warmer than the air at the measurement height. This corresponds to unstable conditions. A traditional indicator of atmospheric stability is the ratio h/L_M, where L_M is the Monin–Obukhov length (see Monin & Yaglom 1971, section 7.2); this ratio is negative (positive) for unstable (stable) cases, and zero for neutral conditions. The ratio h/L_M was about -0.03 for set I, small but not negligible.† For sets II and III, the ground and measurement temperatures differed by less than 0.5 K, and h/L_M was about -0.001 and 0.003, respectively; thus, these two sets correspond essentially to neutrally stable conditions. Set IV, obtained between 2030 and 2100 hours, corresponded to a marginally stable state (the ground was about 1.2 K cooler, and $h/L_M \approx 0.003$). We have analysed all four sets of data, though the focus here is on sets II and III.

In all boundary layer measurements where a gradient in mean temperature is involved, the heating, no matter how small, induces buoyancy at some large scale. In the present instances, the scales affected by buoyancy lie outside the inertial range, and thus slight departures from neutrality have no discernible effect on the scaling results to follow. However, the change in sign of the mean temperature gradient between data sets II and III leads to a change of sign for the skewness of temperature increments. We shall make an additional remark on this aspect in § 3.

Temperature fluctuations were measured by two cold wires placed 5 cm apart in the spanwise direction. They were operated by constant-temperature anemometers built in-house on the basis of a design by Peattie (1987). The operating current was 120 μA; this low value meant that the velocity contamination was minimal. Cold wires were made by etching the silver coating on wires of platinum–10% rhodium alloy made by the Wollaston process, and had a diameter of 0.6 μm and length of the order of 1 mm. The frequency response of the wires was determined to be about 1 kHz, so the low-pass filter was set to that value, and the sampling frequency to 2 kHz. This resolution was adequate for the wind speeds observed. The signals were digitized using a 12-bit A/D analyser.

3. The analytical tools

Some background on the SO(3) decomposition is useful. A velocity structure function tensor of order n depending on a single separation vector $\boldsymbol{r}$ is written as

$$S^{\alpha_1\alpha_2\ldots\alpha_n}(\boldsymbol{r}) = \langle w^{\alpha_1}(\boldsymbol{r}) w^{\alpha_2}(\boldsymbol{r}) \ldots w^{\alpha_n}(\boldsymbol{r}) \rangle, \tag{3.1}$$

† The literature on free convection uses the Rayleigh number as an indication of the strength of convection. If we use the thermal boundary layer height of ≈ 0.5 m as the relevant length scale, we obtain a Rayleigh number of $\approx 5 \times 10^7$.

where

$$w^{\alpha}(\boldsymbol{r}) = u^{\alpha}(\boldsymbol{x}+\boldsymbol{r}) - u^{\alpha}(\boldsymbol{x}), \tag{3.2}$$

and the superscript α denotes the α-component of the velocity in Cartesian coordinates. The rotational invariance of the Navier–Stokes equations suggests that the irreducible representations of the SO(3) symmetry group may be used profitably to decompose a structure function tensor into isotropic and anisotropic parts. We write

$$S^{\alpha_1\ldots\alpha_n}(\boldsymbol{r}) = S^{\alpha_1\ldots\alpha_n}_{j=0}(\boldsymbol{r}) + S^{\alpha_1\ldots\alpha_n}_{j=1}(\boldsymbol{r}) + S^{\alpha_1\ldots\alpha_n}_{j=2}(\boldsymbol{r}) + \cdots, \tag{3.3}$$

and index the various sectors of the SO(3) representation of a given order n by different j values, each of which is orthonormal to every other j, such that the isotropic contribution is contained in the $j = 0$ sector and the higher-order j values contain increasing degrees of anisotropy. The decomposition into isotropic and anisotropic sectors has been implemented for the turbulent velocity field in high-Reynolds-number atmospheric surface layers (Arad *et al.* 1998; Kurien *et al.* 2000; Kurien & Sreenivasan 2001), and for numerical solutions of a channel flow at modest Reynolds numbers (Arad *et al.* 1999*a*; Biferale & Vergassola 2001). The key conclusions are that the components of the tensor corresponding to the different j sectors scale well individually in $r = |\boldsymbol{r}|$, and that the anisotropic sectors decay faster with decreasing r than the isotropic parts, at least up to order 6 of the statistics measured in the atmospheric boundary layer. This means that the isotropic sector makes up the leading term as $r \to 0$. Since the advection–diffusion equation governing a passive scalar is also rotationally invariant, the SO(3) methodology appears to be equally useful for scalar turbulence.

Let us consider the third-order structure function (i.e. $n = 3$ in (2.1)). Homogeneity in the $\hat{\boldsymbol{r}}$-direction implies that the structure function has odd parity in $\boldsymbol{r}$ – that is, it changes sign when $\boldsymbol{r}$ changes sign – as seen below:

$$\begin{aligned} T^{(3)}(-\boldsymbol{r}) &= \langle(\theta(\boldsymbol{x}-\boldsymbol{r}) - \theta(\boldsymbol{x}))^3\rangle \\ &= \langle(\theta(\boldsymbol{x}) - \theta(\boldsymbol{x}+\boldsymbol{r}))^3\rangle \\ &= -\langle(\theta(\boldsymbol{x}+\boldsymbol{r}) - \theta(\boldsymbol{x}))^3\rangle \\ &= -T^{(3)}(\boldsymbol{r}). \end{aligned} \tag{3.4}$$

As already noted, the SO(3) group representation of the structure function for the scalar simplifies to a spherical harmonics representation. We may therefore write

$$T^{(3)}(\boldsymbol{r}) \equiv T^{(3)}(r, \Theta, \Phi) = \sum_{j,m} a_{j,m}(r)\tilde{Y}_{j,m}(\hat{\boldsymbol{r}}), \tag{3.5}$$

where $j = 0\ldots\infty$, and for each j, $m = -j\ldots j$, $r = |\boldsymbol{r}|$, and Θ and Φ are the polar and azimuthal angles, respectively. The $\tilde{Y}_{j,m}(\hat{\boldsymbol{r}})$ are formed from the original spherical harmonics $Y_{j,m}(\hat{\boldsymbol{r}}) = Y_{j,m}(\Theta, \Phi)$ so as to have a real basis (see Kurien *et al.* 2000). The lowest-order basis element $\tilde{Y}_{0,0}(\hat{\boldsymbol{r}})$, being a constant, cannot possess the odd-parity required by (3.4). Thus the expansion begins with the $j = 1$ term and is written as

$$T^{(3)}_{j=1}(\boldsymbol{r}) = (a_{1,0}\cos\Theta + a_{1,1}\sin\Theta\cos\Phi + a_{1,-1}\sin\Theta\sin\Phi)r^{\zeta^{(1)}_3}, \tag{3.6}$$

where the r-dependence has been assumed to obey a scaling law that depends on j (as implied by the superscript of the scaling exponent ζ). As for the velocity field (see Arad, L'vov & Procaccia 1999*b* for theoretical reasons), the scaling exponent for a j-sector is not allowed any dependence on m. From the property of spherical

harmonics that

$$Y_{j,m}(-\hat{\boldsymbol{r}}) = Y_{j,m}(\pi - \Theta, \pi + \Phi) = (-1)^j Y_{j,m}(\Theta, \Phi) = (-1)^j Y_{j,m}(\hat{\boldsymbol{r}}), \tag{3.7}$$

it is clear that the $j = 1$ term has the desired odd-parity. For the two-point measurements of the structure function given by (2.2), $\Phi = \pi/2$, leaving us with just the two terms written below:

$$T^{(3)}_{j=1}(r, \Theta, \Phi = \pi/2) = (a_{1,0} \cos\Theta + a_{1,-1} \sin\Theta) r^{\zeta^{(1)}_3}. \tag{3.8}$$

For $\Theta = \pi/2$, which corresponds to the separation Δ, we have

$$T^{(3)}_{j=1}(\Delta, \Theta = \pi/2, \Phi = \pi/2) = a_{1,-1}\ \Delta^{\zeta^{(1)}_3}, \tag{3.9}$$

showing that the flow-dependent constant $a_{1,-1}$ is given by the non-zero value of the structure function computed at the probe separation distance Δ. A finite contribution to the spanwise structure function is thus not precluded by the lowest-order anisotropy. For $\Theta = 0$ which corresponds to the single probe measurement, equation (3.8) becomes

$$T^{(3)}_{j=1}(r, \Theta = 0, \Phi = \pi/2) = a_{1,0} r^{\zeta^{(1)}_3}. \tag{3.10}$$

We see explicitly the change in sign as Θ changes to π in equation (3.8):

$$T^{(3)}_{j=1}(r, \Theta = \pi, \Phi = \pi/2) = -a_{1,0} r^{\zeta^{(1)}_3}. \tag{3.11}$$

4. Experimental results

We first computed the cross-correlation between signals from the two probes,

$$R(\tau) = \langle \theta_1(t)\theta_2(t + \tau) \rangle, \tag{4.1}$$

and used this as a check on the orientation of the probe separation with respect to mean wind. The peak of the correlation is expected to occur at $\tau = 0$ by homogeneity in the (y, z)-plane. This was so for sets II and IV but the peak was found to be shifted by 5 and 6 sampling units of time for data sets I and III, respectively. A slight misalignment of the probe axis to the mean wind is thus suggested; this effect can be corrected by shifting the signal of one probe with respect to the other by the sampling units equal to the displacement of the peak correlation. This adjustment effectively reorients the probe separation to be orthogonal to the mean wind by setting the shortest spatial separation of the signals to be 4.85 cm and 4.89 cm for data sets I and III, respectively. The time lag τ is henceforth referred to these shifted data.

The temperature signal from each probe was normalized by its r.m.s. value θ' and the structure function computed using this non-dimensional temperature. The two-point structure function computed according to (2.2), where $\theta_i \to \theta_i/\theta_i'$ henceforth, shows the angular variation of the third-order structure function (figure 4). Panels (a) and (b) correspond to data sets II and III, respectively. We display the angular dependence instead of the r-dependence in order to show the unique values attained by the structure function for each Θ between 0 and π radians. Of course, r and Θ are related in our measurements by $r \sin\Theta = \Delta$, giving the same value of r for Θ and $\pi - \Theta$. The structure function appears to assume equal values of opposite sign as $\Theta \to 0$ (corresponding to $\tau \to \infty$) and $\Theta \to \pi$ (corresponding to $\tau \to -\infty$), showing that the $\cos\Theta$ term in (3.8) with a non-zero value of the coefficient $a_{1,0}$ will be needed. It is also the case that the structure function assumes a small non-zero value

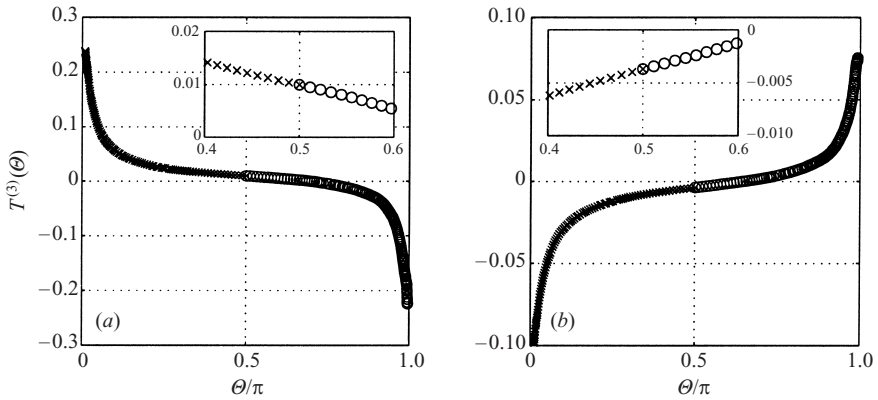

FIGURE 4. The angular dependence of $T^{(3)}$ for the data sets II (*a*) and III (*b*), showing the trend defined in equation (2.2); × indicates $0 < \Theta < \pi/2$ (corresponding to $\tau > 0$) and ○ indicate $\pi/2 < \Theta < \pi$ (corresponding to $\tau < 0$). The insets show that the values of the function at $\pi/2$ are non-zero, positive for data set II and negative for data set III (due to small changes in the stability of the atmosphere). The equivalent range of r covered in these figures varies between 0.05 m and 90 m.

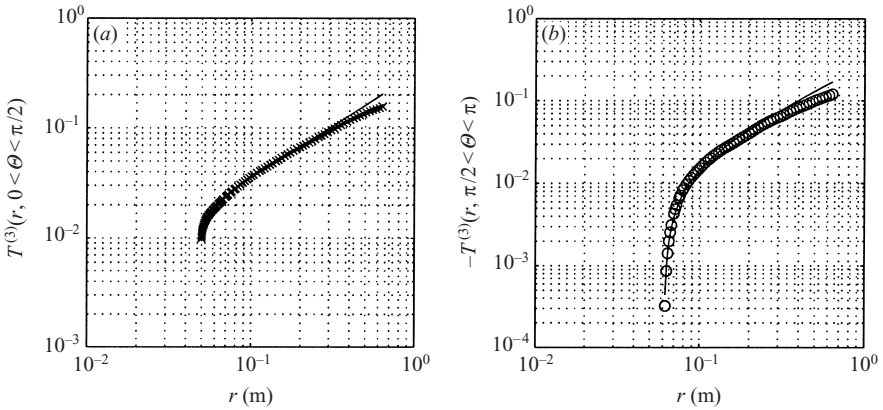

FIGURE 5. Log-log plots of $T^{(3)}(r, \Theta)$ computed from data set II and the fits to the $j = 1$ term given by (3.8): (*a*) $T^{(3)}(r, 0 < \Theta < \pi/2)$ (×); (*b*) $-T^{(3)}(r, \pi/2 < \Theta < \pi)$ (○), since the structure function assumes negative values in this range of angles (see figure 4*a*). The solid lines are the least-square fits within the inertial range. The range of theta used in the fits (corresponding to the smallest r to largest r) are from $\pi/2$ to 0.08π for (*a*), and from $\pi/2$ to 0.92π on (*b*).

at $\Theta = \pi/2$ (see insets of figure 4). This non-zero value corresponding to $\tau = 0$ and $r = \Delta$ indicates that the contribution of the $\sin\Theta$ term in equation (3.8) is necessary, and that its coefficient $a_{1,-1}$ is finite.

The overall change of sign of the structure function between data sets II and III is related to the change in sign of the mean temperature gradient (the ground was slightly hotter than the flow for set II and the reverse was true for III, see § 2). Aside from this sign change, which is consistent with the formula given in Sreenivasan & Tavoularis (1980), all other features are the same for the two sets of data.

To determine the three free parameters $a_{1,0}$, $a_{1,-1}$ and $\zeta_3^{(1)}$ in (3.8), we performed least-squares fits of the equation to $T^{(3)}(\boldsymbol{r})$ computed for the two data sets. The fits to data sets II and III are presented in figures 5 and 6 respectively. Panel (*a*) shows

	$0 < \Theta < \pi/2$			$\pi/2 < \Theta < \pi$		
	$a_{1,0}$	$a_{1,-1}$	$\zeta_3^{(1)}$	$a_{1,0}$	$a_{1,-1}$	$\zeta_3^{(1)}$
I	0.44	0.23	1.00	0.30	0.25	1.00
II	0.30	0.19	1.00	0.28	0.20	1.00
III	−0.17	−0.07	1.00	−0.15	−0.08	1.03
IV	−0.24	−0.01	1.01	−0.20	−0.01	0.98

TABLE 1. Best-fit values of free parameters in (3.8) for data sets I–IV. Changes in stability conditions have no effect on the exponent but change particularly the coefficient $a_{1,-1}$.

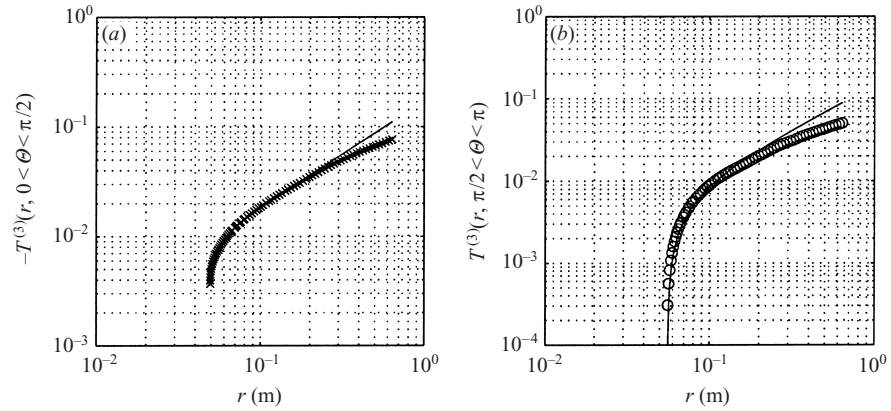

FIGURE 6. Log-log plots of $T^{(3)}(r,\Theta)$ computed from data set III and the fits to the $j = 1$ term given by (3.8): (*a*) $-T^{(3)}(r, 0 < \Theta < \pi/2)$, since the structure function assumes negative values in this range of angles (see figure 4*a*); (*b*) $T^{(3)}(r, \pi/2 < \Theta < \pi)$ (○). The solid lines are the least-square fits within the inertial range. The range of theta used in the fits (corresponding to the smallest r to largest r) are from $\pi/2$ to 0.11π for (*a*), and from $\pi/2$ to 0.89π on (*b*).

the data and the fit for $0 < \Theta < \pi/2$ (corresponding to $\tau > 0$) and panel (*b*) the data and the fit for $\pi/2 < \Theta < \pi$ (corresponding to $\tau < 0$). The variable plotted on the abscissae is now the separation distance r; for each r there is an associated value of Θ given by $r \sin \Theta = \Delta$. The fits were made within the inertial range determined by the linearity of the third-order velocity structure function. The best-fit values of the free parameters, given in table 1 for all sets of data, show some modest differences between the cases $0 < \Theta < \pi/2$ and $\pi/2 < \Theta < \pi$, though the scaling exponent is quite robust.† On the whole, we conclude that the terms corresponding to $j = 1$ describe the third-order structure function rather well.

The skewness of the scalar increment is known to be zero if there are no mean gradients in temperature and velocity (see, for example the measurements in heated grid turbulence of Sreenivasan *et al.* 1980). Hence, a comment on the finite value of $a_{1,-1}$, albeit small compared to $a_{1,0}$, is appropriate. It might be thought that the non-zero value of $a_{1,-1}$ is an indication of persistent spanwise inhomogeneities in the

† The exponent for the third-order structure function, as determined here, is unity within experimental uncertainty. On the other hand, measurements such as those of Meneveau *et al.* (1990) and Moisy *et al.* (2001) show that the exponent for the third moment of the absolute value of temperature differences is about 0.85. The difference between the properties of temperature differences with and without the absolute value is fundamental in ways that will be discussed elsewhere.

flow on inertial-range scales, but it is not hard to show that the presence of shear and mean temperature gradient in one direction can, in fact, set up finite odd moment in a different direction. It appears that (3.7) is general enough to include the case of spanwise shear as well.

The higher-order anisotropy contributions to the third-order structure function coming from $j = 3, 5, \ldots$ may become more important at larger scales, as seen from the 'peel-off' from the fit at large r in figures 5 and 6. However, these terms provide too many additional free parameters ($\geqslant 8$ including exponents) in the fitting procedure, and we have therefore considered it prudent to restrict attention to the leading order.

5. Concluding remarks

Our objective is to understand better the observation that the skewnesses of temperature increments and derivatives show no tendency to isotropy in turbulent flows that possess gradients in mean velocity and temperature. For this purpose, we have explored the SO(3) methodology, the right orthogonal basis here being the spherical harmonics. The main conclusion is that the third-order structure function of temperature is manifestly anisotropic because of odd parity, and isotropy is not its leading behaviour. Only terms with odd j can be present in the spherical harmonics expansion and the lowest order of these, namely $j = 1$, provides adequate fit to experimental data. Thus the skewness can be discussed in terms of the properties of this term.

The present results do not differ from existing empirical wisdom that small scales of a passive scalar retain the memory of large-scale anisotropy. However, they provide a partial answer to the following question: should the persistent skewness be equated with no tendency to isotropy of small-scale scalars? The odd-parity of the skewness does not, by construction, allow it to be the suitable measure for addressing this question. This is similar in spirit to the case presented in Kurien & Sreenivasan (2000) in the context of the anisotropy in high-order velocity structure functions. In that work, the high-order tensor components were chosen so that they were identically zero in the isotropic sector thus directly characterizing the existence of anisotropy in small scales; the fact that anisotropy existed did not automatically imply that there was no approach to isotropy of small-scale turbulence. Such a tendency could be observed by considering the ratios of the isotropic sector to the anisotropic sectors for certain other tensor components of a structure function. Following this line of thought, for the scalars, one has to look for indicators other than the skewness of the scalar derivative or of the increment. For example, structure functions of even order, which are even in parity and so contain a rotationally invariant part, could serve such a purpose; so could the ratios of the isotropic terms to anisotropic terms of even-order objects, as in Celani *et al.* (2000) and in Kurien & Sreenivasan (2001) and Biferale & Vergassola (2001). Alternatively, it is conceivable to phrase the question in terms of the relative magnitudes of the $j = 1$ sector of the third-order structure function and the $j = 0$ sector of the second-order one.

The measurements were made as part of a collaborative effort with the groups of Joe Klewicki and Chris Biltoft. We are grateful to them and their groups for invaluable technical support. We thank Jonathan Burt for his help with measurements and Jörg Schumacher and Detlef Lohse for their comments on the draft. The work was supported by ONR grant 2004093.

REFERENCES

Arad, I., Biferale, L., Mazzitelli, I. & Procaccia, I. 1999*a* Disentangling scaling properties in anisotropic and homogeneous turbulence. *Phys. Rev. Lett.* **82**, 5040–5043.

Arad, I., Dhruva, B., Kurien, S., L'vov, V. S., Procaccia, I. & Sreenivasan, K. R. 1998 Extraction of anisotropic contributions in turbulent flows. *Phys. Rev. Lett.* **81**, 5330–5333.

Arad, I., L'vov, V. S. & Procaccia, I. 1999*b* Correlation functions in isotropy and anisotropic turbulence: The role of the symmetry group. *Phys. Rev.* E **59**, 6753–6765.

Biferale, L. & Vergassola, M. 2001 Isotropy versus anisotropy in small-scale turbulence. *Phys. Fluids* **13**, 2139–2141.

Celani, A., Lanotte, A., Mazzino, A. & Vergassola, M. 2000 Universality and saturation of intermittency in passive scalar turbulence. *Phys. Rev. Lett.* **84**, 2385–2388.

Grossmann, S., von der Heydt, A. & Lohse, D. 2001 Scaling exponents in weakly anisotropic turbulence from the Navier–Stokes equation. *J. Fluid Mech.* **440**, 381–390.

Kurien, S., L'vov, V. S., Procaccia, I. & Sreenivasan, K. R. 2000 Scaling structure of the velocity statistics in atmospheric boundary layers. *Phys. Rev.* E **61**, 407–421.

Kurien, S. & Sreenivasan, K. R. 2000 Anisotropic scaling contributions to high-order structure functions in high-Reynolds-number turbulence. *Phys. Rev.* E **62**, 2206–2212.

Kurien, S. & Sreenivasan, K. R. 2001 Measures of anisotropy and the universal properties of turbulence. In *Les Houches Summer School Proceedings 2000*, pp. 1–60. Springer-EDP.

Lumley, J. L. 1967 Similarity and the turbulent energy spectrum. *Phys. Fluids* **10**, 855–858.

Meneveau, C., Sreenivasan, K. R., Kailasnath, P. & Fan, M. S. 1990 Joint multifractal measures: Theory and applications to turbulence. *Phys. Rev.* A **41**, 894–913.

Mi, J. & Antonia, R.A. 1994 Some checks of Taylor hypothesis in a slightly heated turbulent circular jet. *Expl Therm. Fluid Sci.* **8**, 328–335.

Moisy, F., Willaime, H., Andersen, J. S. & Tabeling, P. 2001 Passive scalar intemittency in low temperature helium flows. *Phys. Rev. Lett.* **86**, 4827–4831.

Monin, A. S. & Yaglom, A. M. 1971 *Statistical Fluid Mechanics*, vol. 1. MIT Press.

Mydlarski, L. & Warhaft, Z. 1998 Three-point statistics and the anisotropy of a turbulent passive scalar. *Phys. Fluids* **10**, 2885–2894.

Peattie, R. 1987 A simple, low-drift circuit for measuring temperatures in fluids. *J. Phys.* E **20**, 565–567.

Shen, X. & Warhaft, Z. 2000 The anisotropy of the small scale structure in high Reynolds number ($R_\lambda \sim 1000$) turbulence shear flow. *Phys. Fluids* **11**, 2976–2989.

Sreenivasan, K. R. 1991 On local isotropy of passive scalars in turbulent shear flows. *Proc. R. Soc. Lond.* A **434**, 165–182.

Sreenivasan, K. R. & Antonia, R. A. 1997 The phenomenology of small-scale turbulence. *Annu. Rev. Fluid Mech.* **29**, 435–472.

Sreenivasan, K. R. & Tavoularis, S. 1980 On the skewness of the temperature derivative in turbulent flows. *J. Fluid Mech.* **101**, 783–795.

Sreenivasan, K. R., Tavoularis, S., Henry, R. & Corrsin, S. 1980 Temperature fluctuations and scales in grid-generated turbulence. *J. Fluid Mech.* **100**, 597–621.

Warhaft, Z. 2000 Passive scalars in turbulent flows. *Annu. Rev. Fluid Mech.* **32**, 203–240.